Ultra-Low-Loss Fiber Bragg Grating Mode Scrambler Design Exploiting Propagation Constant Engineering

Oleksiy Krutko , *Student Member, IEEE*, Rebecca Refaee , Anirudh Vijay , *Member, IEEE*, and Joseph M. Kahn , *Life Fellow, IEEE*

Abstract—Periodic insertion of mode scramblers can reduce the accumulation of group-delay spread and mode-dependent loss in mode-division-multiplexed links. Past effective mode scramblers, however, exhibit too much loss, owing to coupling from guided to unguided modes, specifically cutoff modes. We present a mode scrambler design based on long-period fiber Bragg gratings for links employing graded-index transmission fibers with $D = 12$ guided spatial and polarization modes. In typical graded-index fibers, the guided and lowest-order cutoff modes have nearly equally spaced propagation constants. Hence, a grating will induce coupling not only between all the guided modes but also to the lowest-order cutoff modes, causing high losses. To remedy this problem, we design the mode scrambler transverse refractive index profile to yield equal spacing between the propagation constants of the guided mode groups and a different and larger propagation constant spacing between the highest-order guided modes and the lowest-order cutoff modes. We also ensure that the highest-order guided modes cannot be phase-matched to any other unguided modes by a grating. This enables a uniform grating, obtained by a grid search optimization of the grating parameters, to couple all the guided mode groups with minimal loss. We obtain a design with mode-averaged and mode-dependent loss standard deviations less than 0.027 dB and 0.011 dB, respectively, over the C-band. We perform numerical simulations to study the effect of fabrication errors and show that the choice of grating modulation depth involves a tradeoff between mode scrambler loss and sensitivity of link group-delay spread to fabrication errors.

Index Terms—Bragg gratings, coupling, optical fiber amplifier, optical fiber dispersion, optical fiber devices.

I. INTRODUCTION

POWER-LIMITED long-haul optical communication systems now employ space-division multiplexing (SDM) to meet demands for higher data rates. In current SDM systems, cable capacity is maximized subject to feed-power constraints by using numerous parallel single-mode fibers (SMFs), each carrying a lower power and data rate than in traditional non-SDM systems [1], [2], [3], [4].

Coupled-core multicore fiber (CC-MCF) or multimode fiber (MMF) are alternatives to SMF that can potentially enhance integration and scalability in SDM systems [5], [6] and increase the capacity per fiber. Long-haul links employing MDM in MMF are attractive because they can achieve the highest level of integration [6] and can be efficiently amplified with low mode-dependent gain, while using fewer pump laser diodes per signal mode [7].

Practical implementation of MDM in MMF links requires strong coupling across all signal modes [8]. Strong coupling reduces the standard deviation (STD) of link mode-dependent gain and loss (collectively referred to as MDL), thereby increasing average capacity and reducing outage probability, and reduces group-delay (GD) STD (also known as root-mean-squared GD spread), thereby reducing digital signal processing (DSP) complexity at the receiver. Systems with strong coupling accumulate GD and MDL STDs in proportion to the square root of the propagation length. Strong mode coupling also improves frequency diversity, which further reduces the outage probability [9].

High-capacity long-haul MDM links have often used graded-index (GI) MMFs, owing to their relatively low uncoupled GD STD [10], [11]. In these fibers, the spatial and polarization modes form mode groups. The propagation constants of modes from the same mode group are nearly equal, while those from different mode groups are significantly different. Random perturbations in these fibers cause strong intra-group mode coupling and weak inter-group mode coupling [12].

One way to improve inter-group coupling is to periodically insert mode scramblers in the system [13], [14]. Mode scramblers effect random or deterministic coupling between modes propagating in a fiber. Physical mode scrambler implementations include photonic lanterns [13], distributed multiple point-loads [15], long-period fiber Bragg gratings (LPFGs) [14], [16], and multi-plane light converters (MPLCs) [17]. Fiber-based options like the LPFG-based mode scramblers are especially promising as they are integrable, have low device loss, and can be readily fabricated via ultraviolet laser exposure, CO_2 laser irradiation, electrical discharge, femtosecond laser exposure, mechanical microbends, or etched corrugations [14], [16], [18].

Mode-dependent loss (MDL) and mode-averaged loss (MAL) requirements are stringent for mode scramblers since a signal must pass through tens or hundreds of these devices in a long-haul link [19]. In designing LPFG-based mode scramblers for GI MMF, one must minimize the power coupling from guided modes to unguided modes [14] or cladding modes [19] to ensure low MDL and MAL. There are two main methods reported in the literature. One method involves designing a longitudinal LPFG chirp profile intended to minimize power coupled into the unguided modes [14]. While this approach obtained a mode scrambler design that induced sufficient inter-group coupling, the LPFG losses were too high for practical long-haul MDM links. The other approach minimizes power coupling between the highest-order guided modes and unguided or cladding modes by engineering the propagation constants via the design of the LPFG transverse index profile[1] [19]. Prior studies used a step-index transverse profile [16] or a modified GI transverse profile [19], with features at the core-cladding boundary, to minimize this unwanted power coupling. While the design in [19] successfully reduced the LPFG loss, it provided inter-group coupling insufficient to induce a GD STD proportional to the square root of the number of spans. There is a need for mode scrambler designs providing both low loss and sufficient inter-group coupling.

In this work, we propose an LPFG-based mode scrambler design that jointly optimizes the transverse index profile and longitudinal grating to minimize the LPFG loss while ensuring sufficient coupling to induce square-root accumulation of GD and MDL in multi-span links. As recognized in prior studies, the design of the transverse index profile and grating are highly interdependent [14], [19]. For a uniform grating to effectively couple all the guided modes, the transverse index profile should ensure that the propagation constants of the guided modes are equally spaced. Moreover, to incur low losses, this spacing should significantly differ from the difference between the propagation constants of the highest-order guided modes and any unguided or cladding modes. Instead of engineering propagation constants by adding features to the transverse index profile, we employ the free-form refractive index (RI) optimization method proposed in [20] to systematically design a transverse index profile and use grid search optimization to determine an optimal uniform sinusoidal grating. This design procedure yields LPFG-based mode scrambler designs exhibiting low loss and square-root accumulation of link MDL STD and GD STD. We obtain a design with an MDL STD and MAL less than 0.011 dB and 0.027 dB, respectively, over the C-band. We also perform numerical simulations to study the effect of fabrication errors of the transverse index profile and longitudinal grating on the mode scrambler MDL STD and MAL and link GD STD. We show that the choice of grating modulation depth involves a tradeoff between mode scrambler loss and sensitivity of link GD STD to fabrication errors.

The remainder of the paper is organized as follows. Section II describes modeling modal propagation in LPFGs, modeling

---

[1]We use "transverse index profile" to denote the dependence of the refractive index on the transverse coordinates, which is described by $n(x,y)$ or $n(r)$.
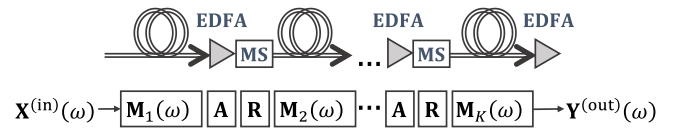

Fig. 1. Diagram of a long-haul MDM transmission link over K fiber spans with periodic amplification and mode scrambling. MS: mode scrambler, EDFA: erbium-doped fiber amplifier.

MDM links with mode scramblers, and the two-step design methodology based on propagation constant engineering. Section III provides the transverse index profile and grating parameters of the designed LPFG-based mode scramblers, quantifies their performance, and evaluates the performance degradation due to various fabrication errors. Sections IV and V are the discussion and conclusion, respectively.

II. Modeling and Design Methodology

This section describes the modeling of LPFGs and MDM links with periodic mode scrambling and presents a methodology for the design of low-loss LPFG-based mode scramblers. The design methodology will later be used to design LPFG-based mode scramblers for a long-haul MDM system design [7] supporting $D = 12$ guided spatial and polarization modes. The term "mode scramblers" hereafter refers to LPFG-based mode scramblers unless noted otherwise.

A. Modeling Methodology

In this subsection, we describe the modeling of propagation in LPFGs and in long-haul MDM links employing periodic mode scrambling.

We consider a long-haul MDM transmission link comprising K MMF spans with periodic amplification and mode scrambling, as shown in Fig. 1. Each MMF span has length L_{span}. In a generalized Jones vector representation, $\mathbf{X}^{(\text{in})}(\omega)$ and $\mathbf{Y}^{(\text{out})}(\omega)$ respectively denote the complex baseband input and output electric field vectors in D spatial and polarization guided modes at an angular frequency ω. The matrices $\mathbf{M}_1(\omega), \mathbf{M}_2(\omega), \ldots, \mathbf{M}_K(\omega)$ denote the $D \times D$ frequency-dependent random transfer matrices for the MMF spans. The $D \times D$ transfer matrix of the link is a product of transfer matrices:

$$\mathbf{M}_{\text{tot}}(\omega) = \mathbf{M}_K(\omega)\mathbf{A}\mathbf{R}\ldots\mathbf{M}_2(\omega)\mathbf{A}\mathbf{R}\mathbf{M}_1(\omega), \quad (1)$$

where $\mathbf{A}$ is a $D \times D$ amplifier transfer matrix and $\mathbf{R}$ is a $D \times D$ mode scrambler transfer matrix describing propagation through the entire mode scrambler. $\mathbf{A}$ and $\mathbf{R}$ depend on wavelength over the C-band, but can be considered frequency-independent over the bandwidth of a typical communication channel. For simplicity in analysis, we assume that there is negligible MDL in the fiber and that the MAL of the fiber is absorbed into $\mathbf{A}$. Therefore, we can model $\mathbf{M}_1(\omega), \mathbf{M}_2(\omega), \ldots, \mathbf{M}_K(\omega)$ as unitary matrices. Loss in $\mathbf{R}$ arises from undesired coupling from guided modes to unguided modes in the scrambling process, and from modal field mismatches between the modes in the
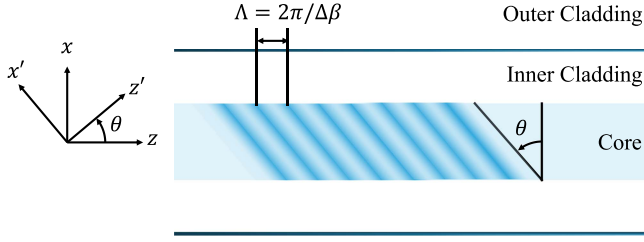
Fig. 2. Diagram of a tilted fiber grating. Λ: grating period, θ: grating tilt. x and z represent the coordinate system of the fiber waveguide, and x' and z' represent the coordinate system of the tilted fiber grating.

transmission fiber and those in the mode scrambler, which are referred to as splicing losses [21].

Fig. 2 shows a diagram of a tilted fiber grating with grating period Λ, tilt angle θ, and length L. The total RI in the mode scrambler can be written as

$$n_{\text{tot}}(x, y, z) = n(r) + \Delta n_{\text{grating}}(x, y, z) \qquad (2)$$

where $n(x, y) = n(r)$ is the transverse index profile of the mode scrambler fiber and $\Delta n_{\text{grating}}(x, y, z)$ is the longitudinal index profile of the mode scrambler grating. $n(r)$ is not necessarily the same as the transverse index profile of the transmission fiber $n_{\text{init}}(r)$. We assume the index modulation of the grating is uniform and present only in the fiber core region, where it is given by

$$
\begin{aligned}
&\Delta n_{\text{grating}}(x, y, z) \\
&= 2\chi \left(1 + \cos\left(\frac{2\pi}{\Lambda \cos\theta} z' \right) \right) P(r) \\
&\approx 2\chi \left(1 + \cos\left(\frac{2\pi}{\Lambda}(z + x\tan\theta) \right) \right) P(r), \qquad (3)
\end{aligned}
$$

where χ is the modulation depth and $P(r) = P(x, y)$ is the radial dependence of the index modulation [14], [22]. Here, $P(r) = 1$ within the core and $P(r) = 0$ outside the core.

Coupled-mode propagation equations model the propagation of guided and unguided modes in the mode scrambler [14], [22], [23]. Solving these, we can obtain $\mathbf{R}$. The guided and unguided mode fields and propagation constants β are computed in a radially resolved cylindrical geometry with a perfectly matched layer and zero termination boundary condition, as in [14], [22]. We assume the outer cladding is index-matched to the inner cladding which can be achieved with an index-matched coating [24]. With an index-matched outer cladding, no discrete cladding modes are supported [14] and inner-outer cladding reflections are suppressed [24].

Using the mode scrambler transfer matrix $\mathbf{R}$, we evaluate the mode scrambler MDL STD and MAL from the eigenvalues of the modal gain operator (MGO) defined as [25]:

$$\mathbf{F}_{\text{MS}} = \mathbf{R}\mathbf{R}^H. \qquad (4)$$

The MGO is Hermitian-symmetric and can be written as $\mathbf{F}_{\text{MS}} = \mathbf{V}_{\text{MS}}\mathbf{\Lambda}_{\text{MS}}^{(g)}\mathbf{V}_{\text{MS}}^H$, where $\mathbf{\Lambda}^{(g)}_{\text{MS}} = \text{diag}\{e^{g_{\text{MS},1}}, \ldots, e^{g_{\text{MS},D}}\}$ is a diagonal matrix of positive eigenvalues representing the optical power gains of the eigenvectors of the MGO, and $\mathbf{V}_{\text{MS}}$ is a

unitary mode scrambler output beam-forming matrix [25]. The mode scrambler MAL is given by

$$\alpha_{\text{MAL}}^{\text{MS}} = \frac{1}{D}\sum_{i=1}^{D} g_{\text{MS},i}, \qquad (5)$$

and the mode scrambler MDL STD is given by

$$\sigma_{\text{MDL}}^{\text{MS}} = \sqrt{\frac{1}{D}\sum_{i=1}^{D}\left(g_{\text{MS},i} - \alpha_{\text{MAL}}^{\text{MS}}\right)^2}. \qquad (6)$$

$\sigma_{\text{MDL}}^{\text{MS}}$, $\alpha_{\text{MAL}}^{\text{MS}}$, and $\mathbf{g}_{\text{MS}}$ are measured in log-power-gain units, and can be converted to decibels by multiplying by $\gamma = 10/\ln 10 \approx 4.34$, i.e., $\sigma_{\text{MDL}}^{\text{MS}}(\text{dB}) = \gamma\sigma_{\text{MDL}}^{\text{MS}}(\text{log power gain})$.

From the total transfer matrix $\mathbf{M}_{\text{tot}}$, we evaluate the overall link GD STD using the GD operator [26]

$$\mathbf{G} = j\frac{\partial \mathbf{M}_{\text{tot}}}{\partial \omega}\mathbf{M}_{\text{tot}}^{-1}(\omega), \qquad (7)$$

where $j = \sqrt{-1}$. The eigenvectors of $\mathbf{G}$ are the principal modes [26], and the eigenvalue of the mth principal mode, $\tau_{\text{tot},i}$, represents its GD. Since we are only interested in the GD STD, we can remove the average GD from each principal mode so that $\sum_{i=1}^{D}\tau_{\text{tot},i} = 0$. Therefore, the link GD STD can be written as

$$\sigma_{\text{GD}}(K) = \sqrt{\frac{1}{D}\text{E}\{\|\boldsymbol{\tau}_{\text{tot}}\|^2\}}, \qquad (8)$$

where $\text{E}\{\cdot\}$ denotes the expected value and $\|\cdot\|$ represents the Euclidean or l^2-norm.

Similarly, we evaluate the overall link MDL STD from the eigenvalues of the MGO for the entire link [25]:

$$\mathbf{F}_{\text{tot}} = \mathbf{M}_{\text{tot}}\mathbf{M}_{\text{tot}}^H. \qquad (9)$$

This link MGO is Hermitian-symmetric and can be written as $\mathbf{F}_{\text{tot}} = \mathbf{V}_{\text{tot}}\mathbf{\Lambda}_{\text{tot}}^{(g)}\mathbf{V}_{\text{tot}}^H$, where $\mathbf{\Lambda}^{(g)}_{\text{tot}} = \text{diag}\{e^{g_{\text{tot},1}}, \ldots, e^{g_{\text{tot},D}}\}$ is a diagonal matrix of positive eigenvalues representing the optical power gains of the eigenvectors of the link MGO, and $\mathbf{V}_{\text{tot}}$ is a unitary matrix describing the link output beam-forming matrix [25]. Assuming the amplifiers precisely compensate for MAL, the real-valued log power gains $\mathbf{g}_{\text{tot}} = [g_{\text{tot},1}, \ldots, g_{\text{tot},D}]^T$ sum to zero, i.e., $g_{\text{tot},1} + \cdots + g_{\text{tot},D} = 0$. The standard deviation of the link MDL σ_{MDL} is a useful quantity for characterizing MDL [25], and is given by

$$\sigma_{\text{MDL}}(K) = \sqrt{\frac{1}{D}\text{E}\{\|\mathbf{g}_{\text{tot}}\|^2\}}. \qquad (10)$$

σ_{MDL} and $\mathbf{g}_{\text{tot}}$ are also measured in log-power-gain units.

B. Transverse Index Profile and Longitudinal Propagation Constants

In this subsection, we first explain key objectives for the modal propagation constants in the mode scrambler fiber: equal spacing between the guided mode groups and a larger spacing between the highest-order guided modes and the unguided modes. We then explain how transverse RI optimization can be used to
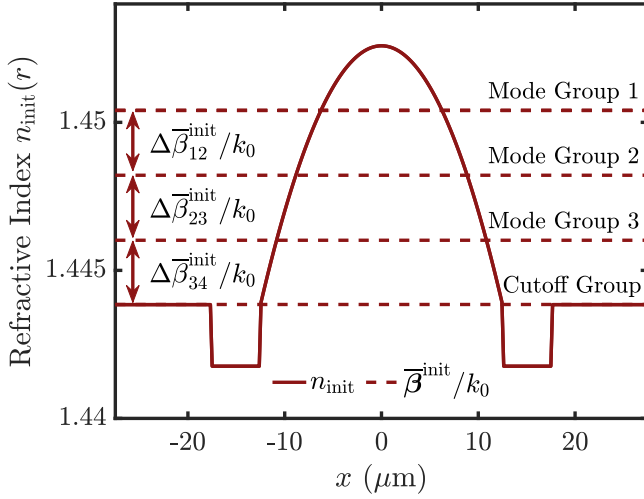
Fig. 3. Transverse index profile $n_{\text{init}}(r)$ of the $D = 12$ trench-assisted GI transmission fiber with 12.5 μm core radius, 5 μm trench width and 125 μm outer diameter used in [7]. The real parts of the mode-group-averaged effective indices $\overline{\boldsymbol{\beta}}^{\text{init}}/k_0$ are indicated by dashed lines, where $k_0 = 2\pi/\lambda$. The mode groups and effective index spacings between mode groups are labeled.

systematically obtain transverse index profiles satisfying these objectives.

Mode coupling by an LPFG is a coherent, phase-matched process [14], [19], [23]. A grating couples two modes most efficiently when

$$\Delta\beta = \frac{2\pi}{\Lambda}, \tag{11}$$

where $\Delta\beta$ is the difference between the modal propagation constants and Λ is the grating period. Considering a simple case in which an MMF supports only two modes, we can evaluate the maximum coupling efficiency η between the modes achievable by a grating:

$$\eta \approx \frac{1}{1 + \left(\frac{\Delta\beta - 2\pi/\Lambda}{C}\right)^2}, \tag{12}$$

where C is the coupling coefficient between the two modes induced by the grating and the self-coupling coefficients are assumed to be negligible [23].

A GI transverse index profile, similar to the transmission fiber in [7], is often proposed for mode scramblers because its modes form mode groups with nearly equally spaced propagation constants, which can therefore all be coupled efficiently by a single uniform grating [14], [19]. For analyzing GI and other similar profiles, we define the real part of the average propagation constant of the ith mode group as $\overline{\beta}_i$ and the propagation constant difference between mode groups i and j as $\Delta\overline{\beta}_{ij} = \overline{\beta}_i - \overline{\beta}_j$.

Fig. 3 shows the transverse index profile $n_{\text{init}}(r)$ and the real part of the mode-group-averaged effective indices $\overline{\boldsymbol{\beta}}^{\text{init}}/k_0$ of the transmission fiber in [7]. The effective indices are obtained by dividing the propagation constants by $k_0 = 2\pi/\lambda$, where λ is the free-space wavelength. For this index profile, the guided modes are $\{LP_{01,x}, LP_{01,y}\}$, $\{LP_{11a,x}, LP_{11a,y}, LP_{11b,x}, LP_{11b,y}\}$, $\{LP_{02,x}, LP_{02,y}, LP_{21a,x}, LP_{21a,y}, LP_{21b,x}, LP_{21b,y}\}$, and

the lowest-order cutoff modes are $\{LP_{12a,x}, LP_{12a,y}, LP_{12b,x}, LP_{12b,y}, LP_{31a,x}, LP_{31a,y}, LP_{31b,x}, LP_{31b,y}\}$.

The guided modes are grouped into $N_g = 3$ mode groups whose propagation constants are nearly equally spaced, i.e., $\Delta\overline{\beta}_{12}^{\text{init}} \approx \Delta\overline{\beta}_{23}^{\text{init}}$, enabling a single uniform grating to couple all the modes. While this is beneficial, a mode scrambler using this transverse index profile will have high loss, since the highest-order guided modes will be coupled efficiently into unguided modes [19]. The most problematic unguided modes are part of the lowest-order cutoff mode group, since $\Delta\overline{\beta}_{34}^{\text{init}} \approx \Delta\overline{\beta}_{12}^{\text{init}} \approx \Delta\overline{\beta}_{23}^{\text{init}}$, the highest-order guided modes are efficiently coupled to them by the grating.

The coupling coefficients between the highest-order guided modes and the lowest-order cutoff modes are larger in magnitude than those between the highest-order guided modes and any other unguided modes. These lowest-order cutoff modes are very nearly linearly polarized, transverse modes similar to the guided modes since their effective indices are close to the cladding index [27]. These modes have significant power in the core and overlap substantially with the guided modes, resulting in efficient coupling [28], [29]. The highest-order guided modes will also couple to other unguided modes, causing additional loss.

To ensure efficient coupling between guided modes by a single grating while minimizing coupling from the highest-order guided modes to unguided modes, we would like to design a transverse index profile that yields propagation constants satisfying the following conditions:

C.1 The propagation-constant spacings between all the guided mode groups should be approximately equal:

$$\Delta\overline{\beta} \approx \Delta\overline{\beta}_{12} \approx \Delta\overline{\beta}_{23} \approx \cdots \approx \Delta\overline{\beta}_{N_g-1\,N_g}.$$

C.2 The propagation-constant spacing between the highest-order guided mode group and the lowest-order cutoff mode group should not equal the spacing between guided mode groups:

$$|\Delta\overline{\beta} - \Delta\overline{\beta}_{N_g\,N_g+1}| \gg 0,$$

where $|\cdot|$ denotes absolute value.

C.3 The highest-order guided mode group should not be efficiently coupled to other unguided modes by a uniform grating that efficiently couples the guided modes:

$$\overline{\beta}_{N_g} - \Delta\overline{\beta} \gg n_{\text{clad}}k_0.$$

It should be noted that simply increasing the core-cladding RI contrast or core radius of a GI fiber will not yield a good design. With this change, the lowest-order cutoff mode group would become guided but still provide a pathway for power coupling out of the original guided modes used to transmit data.

Fig. 4 illustrates how an initial transverse index profile and its propagation constants can be modified to yield desired propagation constants that satisfy conditions C.1-C.3. For clarity, the diagrams in Fig. 4 are not drawn to scale. Fig. 4(a) shows the initial transverse index profile $n_{\text{init}}(r)$ of a trench-assisted GI fiber supporting $N_g = 3$ guided mode groups, while Fig. 4(b) shows the corresponding set of initial mode-group-averaged propagation constants $\boldsymbol{\beta}^{\text{init}}$. Fig. 4(c) shows a set of desired
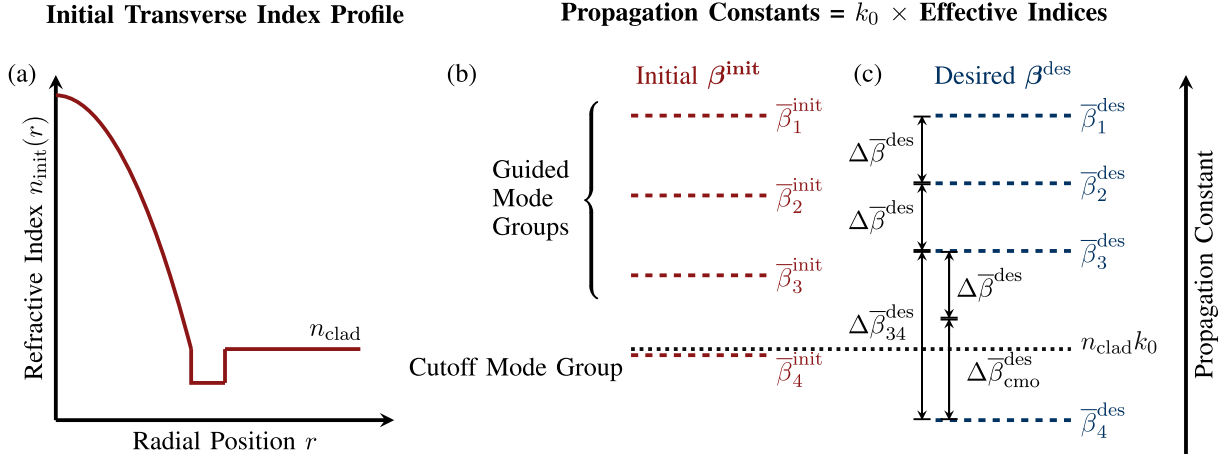
Fig. 4. Propagation constant engineering of LPFG-based mode scramblers: (a) initial transverse index profile of the trench-assisted GI transmission fiber, (b) initial mode-group-averaged propagation constants, and (c) an exemplary set of propagation constants satisfying conditions C.1-3.

mode-group-averaged propagation constants $\boldsymbol{\beta}^{\text{des}}$. In order to satisfy conditions C.1-C.3, $\Delta\overline{\beta}_{34}^{\text{des}}$ is set larger than $\Delta\overline{\beta}^{\text{des}}$, while $\Delta\overline{\beta}_{12}^{\text{des}}$ and $\Delta\overline{\beta}_{23}^{\text{des}}$ are set equal to $\Delta\overline{\beta}^{\text{des}}$, which is smaller than $\Delta\overline{\beta}_{12}^{\text{init}}$ and $\Delta\overline{\beta}_{23}^{\text{init}}$. We have defined an important design parameter related to C.2: the *cutoff mode offset parameter* $\Delta\overline{\beta}_{\text{cmo}}^{\text{des}} = \Delta\overline{\beta}_{34}^{\text{des}} - \Delta\overline{\beta}^{\text{des}}$. We should emphasize that many choices of the desired propagation constants $\boldsymbol{\beta}^{\text{des}}$ can satisfy conditions C.1-C.3.

After choosing the desired propagation constants $\boldsymbol{\beta}^{\text{des}}$, we use the transverse RI optimization method from [20] to find an axially symmetric transverse index profile $n_{\text{des}}(r)$ yielding the desired propagation constants $\boldsymbol{\beta}^{\text{des}}$. We define an objective function based on the squared differences between the actual propagation constants $\boldsymbol{\beta}$ and desired propagation constants $\boldsymbol{\beta}^{\text{des}}$:

$$J = \sum_{i \in \mathcal{M}_{\text{guided}}} \left(\beta_i - \beta_i^{\text{des}}\right)^2 + w_0 \sum_{i \in \mathcal{M}_{\text{cutoff}}} \left(\text{Re}\{\beta_i - \beta_i^{\text{des}}\}\right)^2,$$

$$(13)$$

where w_0 is a weighting factor, $\mathcal{M}_{\text{guided}}$ is the set of guided mode indices, and $\mathcal{M}_{\text{cutoff}}$ is the set of mode indices of the lowest-order cutoff mode group. The modes are indexed in decreasing order of the real part of the propagation constant. We take the real part of the propagation constants of the cutoff modes to remove the imaginary component corresponding to mode attenuation. We use gradient descent to iteratively update the transverse index profile at each radial coordinate r as

$$n(r) \leftarrow n(r) - \mu \frac{\partial J}{\partial n(r)},$$

$$(14)$$

where μ is a step-size parameter that is chosen sufficiently small that perturbative modeling is valid. Details on computing the derivative $\frac{\partial J}{\partial n(r)}$ can be found in [20].

Owing to the high dimensionality of the transverse RI optimization, the desired propagation constants $\boldsymbol{\beta}^{\text{des}}$ may not be achievable by a smooth transverse index profile given a particular initial transverse index profile $n_{\text{init}}(r)$. Therefore, while our choice of the desired propagation constants $\boldsymbol{\beta}^{\text{des}}$ establishes a

goal for the optimization, after convergence, the actual propagation constants $\boldsymbol{\beta}$ may differ from $\boldsymbol{\beta}^{\text{des}}$.

C. Longitudinal Grating Design

This subsection formulates the grid search optimization algorithm used to design the uniform grating. We restrict ourselves to uniform, sinusoidal gratings described by (3). We therefore only need to find a combination of modulation depth χ, grating period Λ, grating length L, and grating tilt angle θ that minimizes the mode scrambler MDL STD $\sigma_{\text{MDL}}^{\text{MS}}$ and MAL $\alpha_{\text{MAL}}^{\text{MS}}$ while ensuring a scaling of the link MDL STD $\sigma_{\text{MDL}}(K)$ and GD STD $\sigma_{\text{GDS}}(K)$ with the square root of the number of spans K:

$$\sigma_{\text{MDL}}(K) = \sqrt{K}\sigma_{\text{MDL}}(1), \qquad (15a)$$

$$\sigma_{\text{GD}}(K) = \sqrt{K}\sigma_{\text{GD}}(1), \qquad (15b)$$

We take $\sigma_{\text{MDL}}(1)$, the MDL STD of a single span, to be the combined MDL STD of a mode scrambler and amplifier pair.

Instead of searching over all possible combinations of the modulation depth, grating period, grating length, and tilt angle, we make several simplifications based on prior studies. We choose a large tilt angle $\theta = 85°$, as in [14], [19], to ensure coupling between modes of different rotational symmetries. We also restrict ourselves to a coarse set of modulation depths. We do not allow the modulation depth to vary freely, because the optimization would tend to minimize the modulation depth, yielding low loss, but making the design overly sensitive to fabrication errors, as discussed below. In summary, our search space comprises a fixed tilt angle, a coarse grid of modulation depths and a fine grid of grating periods and grating lengths.

To evaluate each grating design, we use the following objective function:

$$\sum_{\lambda} \left(w_1 \Phi\left(\frac{\sigma_{\text{GD},\lambda}(K)}{\sqrt{K}\sigma_{\text{GD},\lambda}(1)}\right) + w_2 \Phi\left(\frac{\sigma_{\text{MDL},\lambda}(K)}{\sqrt{K}\sigma_{\text{MDL},\lambda}(1)}\right) \right.$$

$$\left. + w_3 \sigma_{\text{MDL},\lambda}^{\text{MS}} + w_4 \alpha_{\text{MAL},\lambda}^{\text{MS}} \right), \qquad (16)$$

where $\Phi(x)$ is defined as

$$\Phi(x) = \begin{cases} 0, & x \le 1 \\ 50(x-1)^2, & x > 1 \end{cases}, \qquad (17)$$

the w_i are weighting parameters, and the λ are the wavelengths at which the grating design is evaluated. The terms with $\Phi(x)$ penalize designs that do not yield link MDL STD and GD STD accumulation with the square root of the number of spans K. We find that evaluating the objective function at only three wavelengths, 1530, 1550, and 1565 nm, is sufficient to obtain good performance over the entire C-band.

III. RESULTS

In this section, we use our proposed design strategy to design LPFG-based mode scramblers for the long-haul MDM link architecture proposed in [7], which supports $D = 12$ guided spatial and polarization modes.

A. Transverse Index Profile

In this subsection, we use the transverse RI optimization scheme described in Section II-B to obtain multiple designs and provide intuitive explanation of the resulting transverse index profiles.

The trench-assisted GI transmission fiber in [7] is used as the initial transverse index profile $n_{\text{init}}(r)$ in our optimization. This profile is a good starting point because the guided mode groups have equal propagation constant spacing and the resulting optimized profiles will remain similar to the initial transmission fiber, leading to low splicing loss. We set $\overline{\beta}_1^{\text{des}} = \overline{\beta}_1^{\text{init}}$, $\Delta\overline{\beta}^{\text{des}} = \Delta\overline{\beta}_{12}^{\text{des}} = \Delta\overline{\beta}_{23}^{\text{des}} = \Delta\overline{\beta}_{12}^{\text{init}} - k_0 \times 10^{-4}$ and $w_0 = 0.05$, and vary the cutoff mode offset parameter $\Delta\overline{\beta}_{\text{cmo}}^{\text{des}} = \Delta\overline{\beta}_{34}^{\text{des}} - \Delta\overline{\beta}^{\text{des}}$ from $0.4k_0 \times 10^{-4}$ to $4k_0 \times 10^{-4}$. The weight parameter w_0 is small to ensure the optimization prioritizes equal spacing between the guided mode group propagation constants (condition C.1). In each gradient descent iteration, the transverse index profile is only allowed to vary within the core region, $r < 12.5$ μm, and is smoothed by a Gaussian smoothing filter. About 400 iterations are needed to achieve convergence with a step size $\mu = 5 \times 10^{-6}$.

Fig. 5 shows multiple transverse index profiles obtained by transverse RI optimization for various normalized cutoff mode offset values. Since the guided mode group spacings are not precisely equal for the optimized transverse profiles, the cutoff mode offset is taken as the difference between the propagation constant spacing of the highest-order guided mode group and the lowest-order cutoff mode group with the average propagation constant spacing of the guided mode groups:

$$\Delta\overline{\beta}_{\text{cmo}} = \overline{\beta}_3 - \overline{\beta}_4 - \frac{\overline{\beta}_1 - \overline{\beta}_3}{2} = \Delta\overline{\beta}_{34} - \frac{\Delta\overline{\beta}_{13}}{2}. \qquad (18)$$

The cutoff mode offsets are normalized by k_0 to be expressed in terms of effective indices. The larger the cutoff mode offset is chosen to be, the more the optimized RI profile differs from the initial profile. Compared to the initial profile, the optimized profiles have higher RI for 5.2 μm $< r < 8.5$ μm. Depending on the cutoff mode offset parameter, the optimized profiles have a
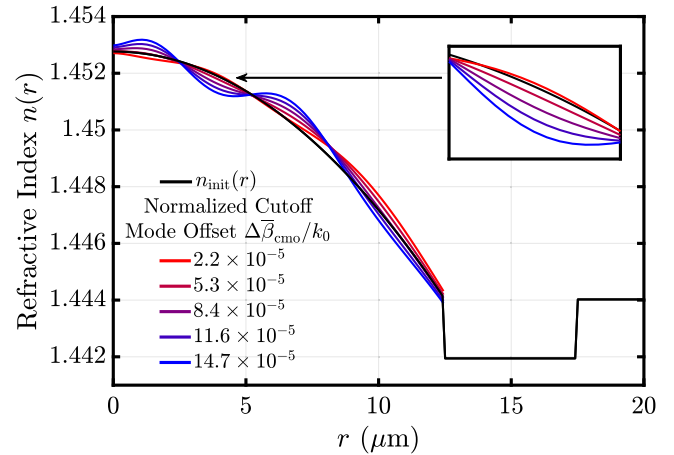

Fig. 5. Optimized transverse index profiles $n(r)$ for various normalized cutoff mode offset values. The initial transverse index profile $n_{\text{init}}(r)$ is of the trench-assisted GI fiber shown in Fig. 3. The optimization only varies $n(r)$ in the core region, $r < 12.5$ μm.

higher RI for 0 μm $< r < 2.4$ μm and a lower RI for 8.5 μm $< r < 12.5$ μm or vice versa. The optimized profiles take this form because, in each optimization step, the RI update at a specific spatial coordinate is a weighted linear combination of the modal intensities at that coordinate, where the weights are the relative errors between the actual and desired propagation constants [20].

We use this insight to study the optimized transverse index profile with normalized cutoff mode offset equal to 14.7×10^{-5} marked by the pure blue line in Fig. 5. Fig. 6(a) and (c) show, respectively, the combined intensities of the mode groups[2] and the RI update in the 20-th iteration. Fig. 6(b) and (d) show, respectively, the combined intensities of the mode groups and the RI update in the 100-th iteration. Owing to the small weight value $w_0 = 0.05$, the optimization initially prioritizes obtaining $\overline{\beta}_1^{\text{des}} = \overline{\beta}_1^{\text{init}}$ and $\Delta\overline{\beta}_{12}^{\text{des}} = \Delta\overline{\beta}_{23}^{\text{des}} = \Delta\overline{\beta}_{12}^{\text{init}} - k_0 \times 10^{-4}$. This first stage takes approximately 60 iterations to complete. To keep $\overline{\beta}_1^{\text{des}} = \overline{\beta}_1^{\text{init}}$, the RI update overlaps minimally with the combined modal intensity of the first mode group. To obtain $\Delta\overline{\beta}_{12}^{\text{des}} = \Delta\overline{\beta}_{23}^{\text{des}} = \Delta\overline{\beta}_{12}^{\text{init}} - k_0 \times 10^{-4}$, the RI update overlaps maximally with the combined modal intensities of the second and third mode groups. In the second stage, the optimization attempts to obtain a larger cutoff mode offset while maintaining the desired guided mode propagation constants. Therefore, the RI update is typically negative at radii where the overall intensity of the cutoff mode group is largest, and is typically positive at radii where the overall intensity of the cutoff mode group is smallest.

As mentioned at the end of Section II-B, the optimized transverse index profiles may not achieve the set of desired propagation constant β^{des}. For each of the optimized transverse index profiles, we evaluate the cutoff mode offset and the guided mode difference, given by:

$$\Delta\overline{\beta}_{\text{gmd}} = |\Delta\overline{\beta}_{12} - \Delta\overline{\beta}_{23}|. \qquad (19)$$

[2]The combined intensity of a mode group is obtained by incoherently summing the intensities of its constituent modes.
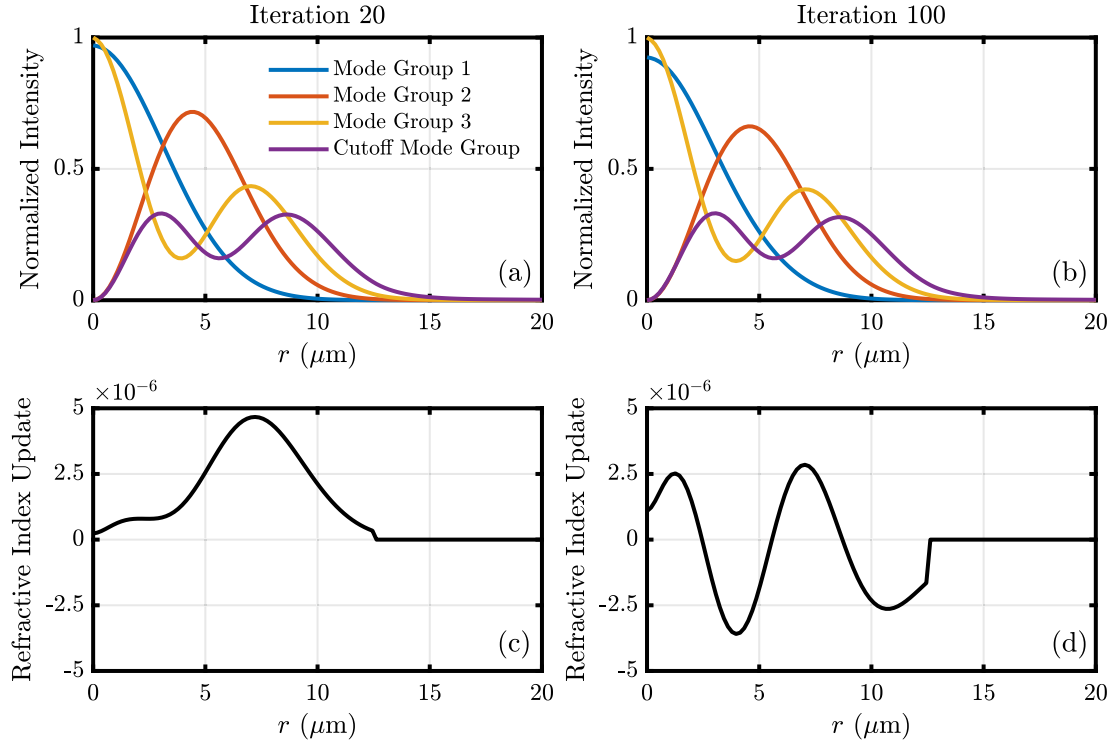
Fig. 6. Snapshots of the combined mode group intensities and transverse RI updates at iterations 20 and 100. Combined mode group intensities (a) and RI update (c) at iteration 20 are representative of the first stage of the transverse RI optimization (first ~ 60 iterations), during which the optimization attempts to obtain $\overline{\beta}_1^{\text{des}} = \overline{\beta}_1^{\text{init}}$ and $\Delta\overline{\beta}_{12}^{\text{des}} = \Delta\overline{\beta}_{23}^{\text{des}} = \Delta\overline{\beta}_{12}^{\text{init}} - k_0 \times 1 \times 10^{-4}$. Combined mode group intensities (b) and RI update (d) at iteration 100 are representative of the second stage of the transverse RI optimization (after ~ 60 iterations), during which the optimization obtains a normalized cutoff mode offset of 14.7×10^{-5}.
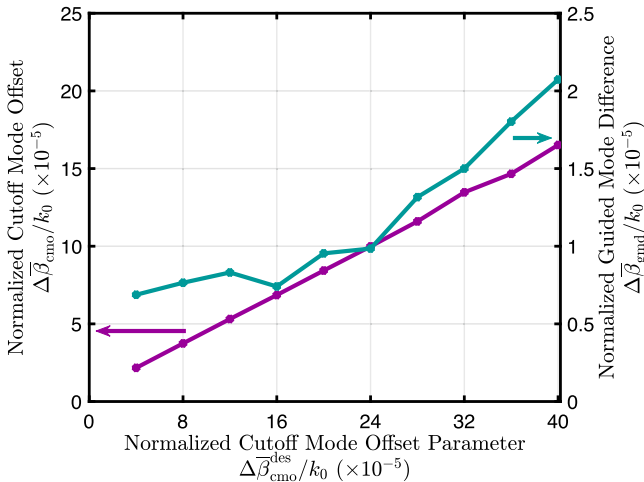

Fig. 7. Normalized cutoff mode offset (purple) and normalized guided mode spacing difference (teal) as a function of the normalized cutoff mode offset parameter. Each of the quantities is normalized by k_0 to be expressed in terms of effective indices.

A transverse index profile with a large guided mode difference $\Delta\overline{\beta}_{\text{gmd}}$ could prevent a grating from achieving sufficient intergroup coupling.

Fig. 7 shows the normalized guided mode difference and normalized cutoff mode offset as a function of the normalized cutoff mode offset parameter. Each of the quantities is normalized by k_0. As the cutoff mode offset parameter increases, the

cutoff mode offset and the guided mode spacing difference also increase. These optimized transverse index profiles trade off between conditions C.1 and C.2; profiles with larger cutoff mode offsets yield larger guided mode propagation constant spacing differences. As a result, the cutoff mode offset obtained is not equal to the cutoff mode offset parameter. In the optimized designs, their ratio is approximately 0.45. The optimized profiles satisfy condition C.3: $\overline{\beta}_{N_g} - \Delta\overline{\beta} \approx n_{\text{clad}}k_0 + 2k_0 \times 10^{-4} \gg n_{\text{clad}}k_0$.

B. Longitudinal Grating and Mode Scrambler Performance

In this subsection, we obtain mode scrambler designs by using the grid search optimization algorithm described in Section II-C to find a combination of grating parameters for each of the optimized transverse index profiles found in Section III-A. We compute the losses of these mode scramblers to find the design with the lowest loss. We evaluate the link GD STD and MDL STD for a link using the design with the lowest loss.

We use the numerical mode solver described in Section II-A to compute the electric field profiles and propagation constants of the guided and unguided modes. We use Sellmeier equation fitting parameters to capture the material dispersion for fused silica in the core and cladding [30]. We find that to accurately model the mode scrambler losses, it is sufficient for the coupled-mode propagation equations to use the 50 unguided modes with the closest phase match and largest coupling coefficients to the highest-order guided modes. We also evaluate the group delays
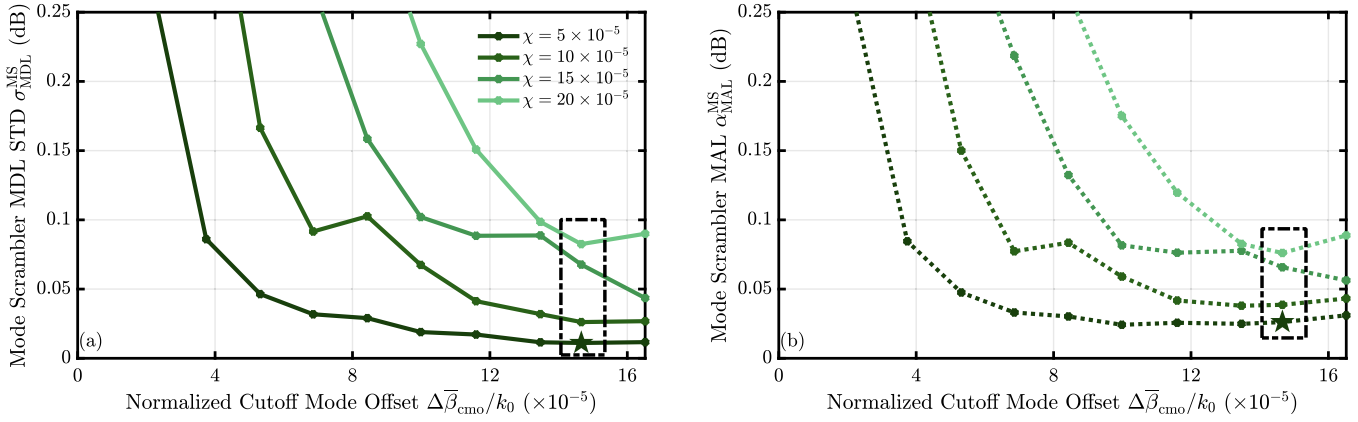
Fig. 8. (a) Maximum mode scrambler MDL STD $\sigma_{\mathrm{MDL}}^{\mathrm{MS}}$ (solid) over the C-band and (b) maximum mode scrambler MAL $\alpha_{\mathrm{MAL}}^{\mathrm{MS}}$ (dashed) over the C-band as a function of the normalized cutoff mode offset. The cutoff mode offset $\Delta\overline{\beta}_{\mathrm{cmo}}$ is normalized by k_0 to be expressed in terms of effective index. The mode scrambler design with the lowest MDL STD is marked on the plots by stars. The mode scrambler designs enclosed by the dashed black rectangles are studied for fabrication sensitivity. The legend in (a) also applies to (b).

per unit length of the guided modes for use in the multisection model of the link.

The link MDL STD and GD STD are evaluated for a 100-span link with identical mode scramblers and amplifiers after every span. Each span is of length $L_{\mathrm{span}} = 50$ km and is modeled as a concatenation of 50 shorter sections with random block unitary coupling matrices to simulate strong intra-group coupling and no inter-group coupling. The assumption of no inter-group coupling is pessimistic, as it places the burden of inter-group coupling on the mode scrambler. The frequency dependence of each shorter section is captured to first order by the uncoupled modal GDs. The amplifier transfer matrix $\mathbf{A}$ is assumed to be diagonal with an MDL STD of 0.1 dB and wavelength variation taken from [7].

Using a grid search, we find optimal grating parameters for values of the modulation depth χ equal to 5×10^{-5}, 10×10^{-5}, 15×10^{-5}, or 20×10^{-5} and tilt angle $\theta = 85°$ for each optimized transverse index profile in Section III-A. In the grid search, the grating period Λ is varied between 743 μm and 749 μm, while the grating length L is varied between 0cm and 10cm. Each design is evaluated using the objective function in (16) with weights set to 1 and evaluation wavelengths 1530, 1550 and 1565 nm.

Fig. 8(a) and (b) show, respectively, the maximum mode scrambler MDL STD $\sigma_{\mathrm{MDL}}^{\mathrm{MS}}$ and mode scrambler MAL $\alpha_{\mathrm{MAL}}^{\mathrm{MS}}$ over the C-band, as a function of the normalized cutoff mode offset. Stars mark the mode scrambler with the lowest MDL STD. In these figures, dashed black rectangles enclose four mode scrambler designs with the same transverse index profile but different grating parameters. These will be used in studying the sensitivity of mode scrambler performance to fabrication errors in Section III-C.

As the cutoff mode offset is increased, the mode scrambler MDL STD and MAL decrease rapidly before leveling off. Once the cutoff mode offset value becomes sufficiently high, splicing loss and coupling to unguided modes other than the lowest-order cutoff modes become the dominant losses. Further increasing the cutoff mode offset beyond this threshold leads to an increase in MAL. For designs with modulation depths 5×10^{-5} and
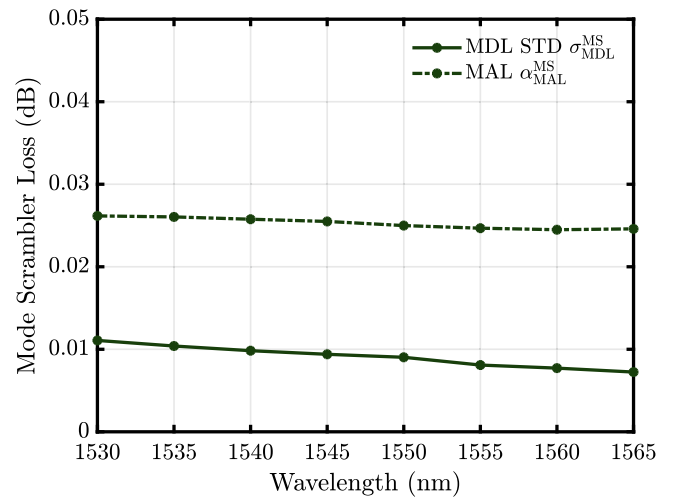

Fig. 9. Mode scrambler MDL STD $\sigma_{\mathrm{MDL}}^{\mathrm{MS}}$ and MAL $\alpha_{\mathrm{MAL}}^{\mathrm{MS}}$ over the C-band of the mode scrambler with the lowest MDL STD, indicated by stars in Fig. 8.

10×10^{-5}, the normalized cutoff mode offset threshold value is about 13.4×10^{-5}. For each optimized transverse index profile, the MDL and MAL reach minimum values at the lowest modulation depth value of $\chi = 5 \times 10^{-5}$. The minimum MDL STD of 0.011 dB is achieved by the transverse index profile with normalized cutoff mode offset value equal to 14.7×10^{-5}, indicated by a star. The minimum MAL value of 0.026 dB is achieved by the transverse index profile with normalized cutoff mode offset equal to 13.4×10^{-5}.

Fig. 9 shows the wavelength dependence of the mode scrambler MDL STD $\sigma_{\mathrm{MDL}}^{\mathrm{MS}}$ and mode scrambler MAL $\alpha_{\mathrm{MAL}}^{\mathrm{MS}}$ for the design with the least loss, which is indicated by stars in Fig. 8. The MDL STD and MAL weakly vary with wavelength, trending to slightly lower loss at longer wavelengths. Fig. 10(a) and (b) plot, respectively, the link MDL STD σ_{MDL} and link GD STD σ_{GD} as a function of the number of spans. The black dashed line corresponds to a link without mode scrambling and only intra-group coupling. Without mode scrambling, the GD STD
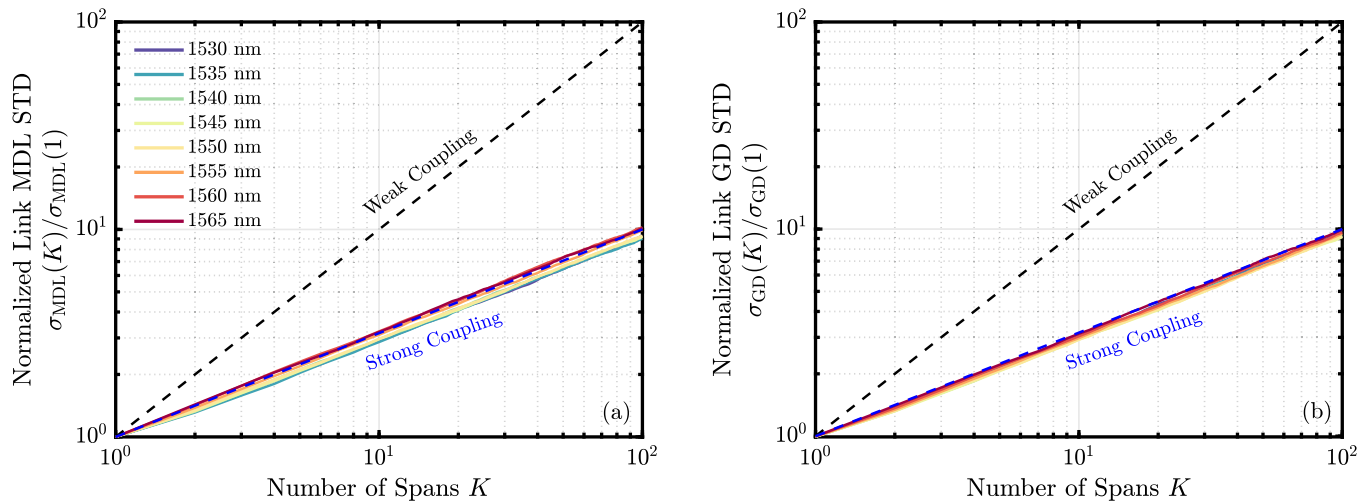
Fig. 10. (a) Normalized link MDL STD and (b) normalized link GD STD as a function of number of spans at multiple wavelengths in the C-band in a long-haul MDM link using the mode scrambler with the lowest mode scrambler MDL STD $\sigma_{\text{MDL}}^{\text{MS}}$. The link GD STD $\sigma_{\text{GD}}(K)$ is normalized by the one-span GD STD $\sigma_{\text{GD}}(1)$. Similarly, the MDL STD $\sigma_{\text{MDL}}(K)$ is normalized by the per-device (amplifier and mode scrambler) MDL STD $\sigma_{\text{MDL}}(1)$. The black dashed line (weak coupling) simulates a link with no mode scramblers and only intra-group coupling. The blue dashed line (strong coupling) simulates a link with strong random coupling. The legend in (a) also applies to (b).

TABLE I
OPTIMAL GRATING PARAMETERS FOR THE OPTIMIZED TRANSVERSE REFRACTIVE INDEX PROFILE

Modulation depth χ	Grating period Λ (μm)	Grating length L (cm)	Mode scrambler MAL $\alpha_{\text{MAL}}^{\text{MS}}$ (dB)[1]	Mode scrambler MDL STD $\sigma_{\text{MDL}}^{\text{MS}}$ (dB)[1]
5×10^{-5}	743.1	4.42	0.011	0.026
10×10^{-5}	746.0	2.12	0.026	0.039
15×10^{-5}	749.0	1.98	0.068	0.066
20×10^{-5}	747.8	1.01	0.082	0.076

The grating parameters of the mode scrambler designs enclosed by the dashed rectangular boxes in Fig. 8. The transverse index profile has a normalized cutoff mode offset of 14.7×10^{-5} and the grating has a tilt angle of $85°$.
[1]Maximum over C-band.

and MDL STD are proportional to the number of spans. The blue dashed line corresponds to a link with strong random coupling. The plots in Fig. 10(a) and (b) verify that the mode scrambler design results in the link MDL STD and the link GD STD scaling with the square root of the number of spans over the entire C-band.

Table I provides optimal values of the grating period Λ and grating length L, and maximum values of the mode scrambler MDL STD $\sigma_{\text{MDL}}^{\text{MS}}$ and MAL $\alpha_{\text{MAL}}^{\text{MS}}$ over the C-band, for mode scramblers with normalized cutoff mode offset value 14.7×10^{-5}, for several different values of the grating modulation depth χ. As the modulation depth χ is increased, the grid search selects designs with longer grating periods and shorter grating lengths. The preference for longer grating periods at higher modulation depths can be understood from (12). A larger modulation depth results in larger coupling coefficients between modes, thereby increasing the maximum coupling efficiencies between the modes, including unguided modes. Since sufficient inter-group coupling is already achievable for a modulation depth χ equal to 5×10^{-5}, any further increase in coupling efficiency only results in more loss to unguided modes [23]. The grid search reduces loss by using longer grating periods to increase the phase mismatch between the highest-order guided modes and unguided modes. Also, the grid search prefers

shorter grating lengths L for higher modulation depths because the necessary inter-group coupling can occur within a shorter distance.

In Section III-A, we noted that the optimized transverse index profiles with larger cutoff mode offsets yield larger propagation constant spacing differences between the guided mode groups. While it was initially unclear if profiles with large cutoff mode offsets would provide net performance benefits, Figs. 8 and 10 clearly demonstrate the benefits of this approach since mode scramblers using these profiles can achieve the lowest losses and obtain sufficient inter-group coupling to meet the link MDL STD and GD STD targets.

C. Sensitivity to Fabrication Errors

In this subsection, we analyze the impact of fabrication errors on mode scrambler performance.

Deviations in the transverse or longitudinal index profiles impact the power coupling between modes. In an extreme case, these deviations can lead to insufficient inter-group coupling and/or increased coupling to unguided modes. From (12), we can see that the sensitivity of coupling efficiency to phase mismatch can be reduced by increasing the coupling coefficient. Therefore, we anticipate that the inter-group coupling in mode scramblers
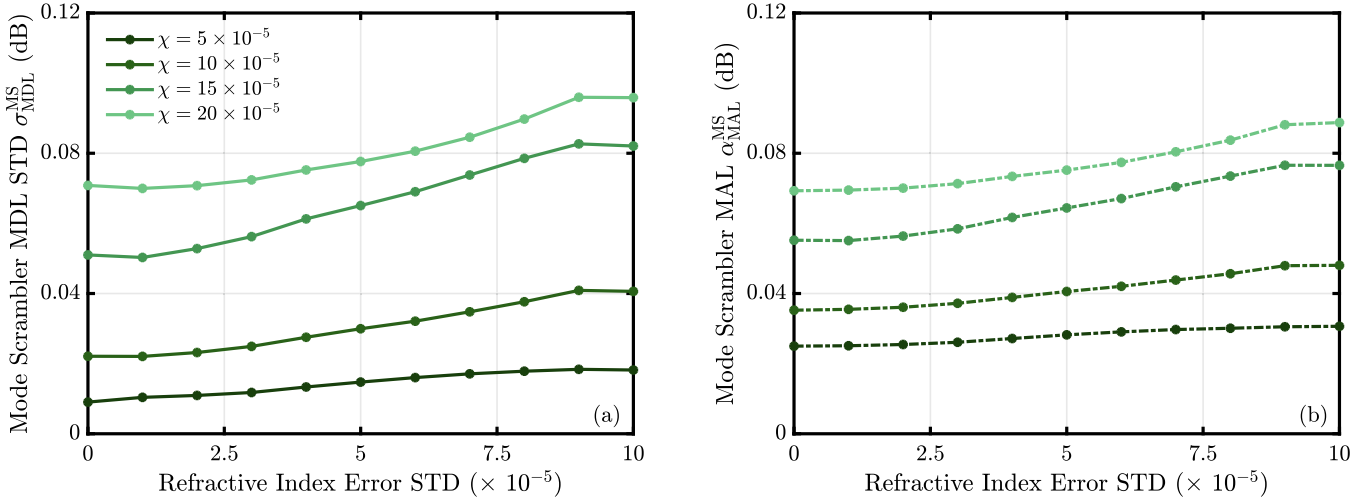
Fig. 11.   (a) Average mode scrambler MDL STD $\sigma_{\mathrm{MDL}}^{\mathrm{MS}}$ and (b) average mode scrambler MAL $\alpha_{\mathrm{MAL}}^{\mathrm{MS}}$ as a function of the transverse RI error STD. The transverse index profile for all the mode scramblers has a normalized cutoff mode offset of 14.7×10^{-5}. The grating parameters are from Table I.

with higher modulation depths will be less affected by transverse and longitudinal index profile errors.

We study the mode scramblers enclosed in dashed rectangles in Fig. 8. These mode scrambler designs all use the same transverse index profile but use different grating parameters, as given in Table I. We first analyze the sensitivity of mode scrambler loss to transverse index profile perturbations while keeping the grating parameters unchanged. As in [20], we generate random perturbations of the form

$$\delta n(r) = \sum_{i=1}^{N} A_i \cos\left(2\pi f_i r + \phi_i\right) + B_i \sin\left(2\pi f_i r + \theta_i\right), \tag{20}$$

where N is the number of sinusoids used in the expansion of the random deviation, f_i are the spatial frequencies, A_i and B_i are the amplitudes of the spatial frequencies, and ϕ_i and θ_i are random phase offsets. Random deviations are produced with $N = 5$ and f_i linearly spaced from 5×10^4 m^{-1} to 25×10^4 m^{-1}. ϕ_i and θ_i are uniformly distributed from 0 to 2π radians and A_i and B_i are taken from a zero-mean Gaussian distribution with unit variance, $A_i, B_i \sim \mathcal{N}(0, 1)$. A_i and B_i are then scaled so that $\delta n(r)$ has a desired RI error STD. For each RI error STD, we simulate 1000 deviated transverse index profiles with independently generated $\delta n(r)$.

Fig. 11 plots the average mode scrambler MDL STD and average mode scrambler MAL as a function of the RI error STD at 1550 nm. The mode scrambler MDL STD and MAL increase with increasing RI error STD. Even with an RI error STD of 10×10^{-5}, all mode scramblers maintain MDL STDs and MALs below 0.1 dB. We attribute this robustness to the large cutoff mode offset value of 14.7×10^{-5}. We expect that only an improbable perturbation with that STD can significantly increase the loss.

While the losses of the optimized mode scramblers are robust to errors in the transverse index profile, these errors can also impact the inter-group coupling which, in turn, can affect the link

GD STD and MDL STD. Errors in the longitudinal index profile can similarly impact the link GD STD and MDL STD. Here, we analyze how random or systematic errors in six fabrication error scenarios impact the link GD STD of an MDM link comprising $K = 100$ spans. We show that mode scramblers with higher modulation depths are substantially more robust to both random and systematic errors, as expected from (12). The six fabrication error scenarios are:

1) *Random transverse index profile errors:* each mode scrambler's index profile $n(r)$ is subject to an independent realization of an error $\delta n(r)$ computed from (20) using the same parameters as in the error study above.

2) *Random grating period errors:* each mode scrambler's grating period Λ is subject to an independent realization of an error $\delta \Lambda \sim \mathcal{N}(0, \sigma_\Lambda^2)$, where σ_Λ is the grating period error STD.

3) *Random modulation depth errors:* each mode scrambler's grating modulation depth χ is subject to an independent realization of an error $\delta \chi \sim \mathcal{N}(0, \sigma_\chi^2)$, where σ_χ is the modulation depth error STD.

4) *Systematic transverse index profile errors:* the index profile $n(r)$ in all mode scramblers is subject to an identical realization of an error $\delta n(r)$ computed from (20) using the same parameters as in the error study above.

5) *Systematic grating period errors:* the grating period Λ in all mode scramblers is subject to an identical error $\delta \Lambda$, which is swept through the range $[-\delta_\Lambda, \delta_\Lambda]$, where δ_Λ is the maximum grating period error.

6) *Systematic modulation depth errors:* the modulation depth χ in all mode scramblers is subject to an identical error $\delta \chi$, which is swept through the range $[-\delta_\chi, \delta_\chi]$, where δ_χ is the maximum modulation depth error.

For each scenario with random errors, we simulate 1000 random realizations of the $K = 100$ span link and evaluate the average link GD STD. For the scenario with systematic transverse index errors, we simulate 1000 random realizations of the index error $\delta n(r)$ and evaluate the worst-case link GD
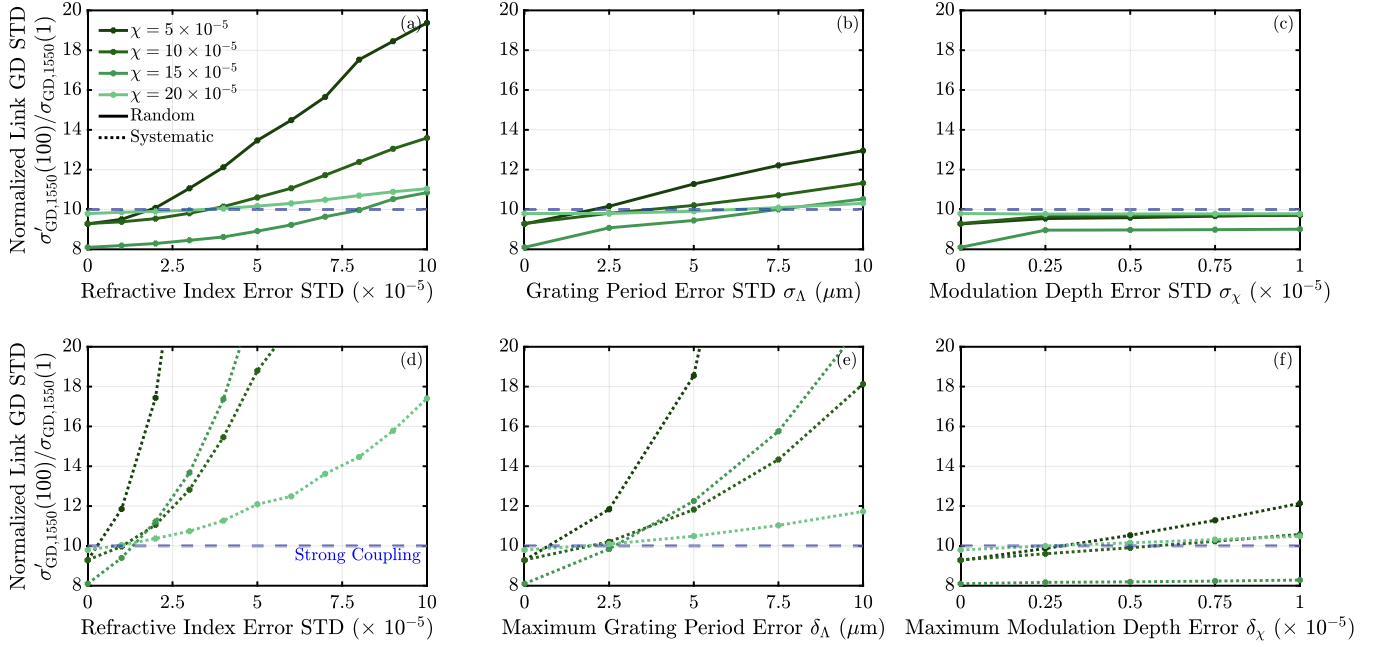
Fig. 12. Impact of random or systematic mode scrambler fabrication errors on the GD STD of an MDM link with $K = 100$ spans. (a) Average normalized link GD STD due to random transverse RI errors as a function of RI error STD. (b) Average normalized link GD STD due to random grating period errors as a function of grating period error STD σ_Λ. (c) Average normalized link GD STD due to random modulation depth errors as a function of modulation depth error STD σ_χ. (d) Worst-case normalized link GD STD due to systematic transverse RI errors as a function of RI error STD. (e) Worst-case normalized link GD STD due to systematic grating period errors as a function of maximum grating period error. (f) Worst-case normalized link GD STD due to systematic modulation depth errors as a function of maximum modulation depth error. Worst-case normalized GD STDs due to random errors are indicated by solid lines and worst-case normalized GD STDs due to systematic errors are indicated by dashed lines. In all panels, the GD STD $\sigma'_{GD}(K)$ is normalized by the one-span GD STD $\sigma_{GD}(1)$. The dashed blue line indicates the GD STD after $K = 100$ spans of a link with strong random coupling. The transverse index profile for all the mode scramblers has a normalized cutoff mode offset of 14.7×10^{-5}. The grating parameters are from Table I.

STD. For the scenarios with systematic errors in either modulation depth or grating period, we evaluate the worst-case link GD STD within the studied range. We use σ'_{GD} to represent either the average link GD STD or the worst-case link GD STD.

We first consider the fabrication error scenarios with random errors shown in Fig. 12(a) to (c). Fig. 12(a) shows the average normalized link GD STD $\sigma'_{GD}(100)/\sigma_{GD}(1)$ due to random RI errors as a function of the RI error STD at 1550 nm. The dashed blue line indicates the link GD STD after $K = 100$ spans of a link with GD STD proportional to the square root of the number of spans. As expected from (12), the link GD STD of mode scramblers with higher modulation depths are more robust to transverse index profile errors. At the highest RI error STD, the average link GD STD increases by 110% for the design with modulation depth $\chi = 5 \times 10^{-5}$, while only increasing by 13% for the design with modulation depth $\chi = 20 \times 10^{-5}$.

Fig. 12(b) shows the average normalized link GD STD $\sigma'_{GD}(100)/\sigma_{GD}(1)$ due to random grating period errors as a function of grating period error STD σ_Λ at 1550 nm. Similarly, mode scramblers with higher modulation depths are more robust to grating period errors. At the highest grating error STD, the average link GD STD increases by 90% for the design with modulation depth $\chi = 5 \times 10^{-5}$, while only increasing by 10% for the design with modulation depth $\chi = 20 \times 10^{-5}$. We believe that the grating period errors considered here are pessimistic, since short-period fiber gratings with grating periods on the order of 1 μm are commercially available.

Fig. 12(c) shows the average normalized link GD STD $\sigma'_{GD}(100)/\sigma_{GD}(1)$ due to random modulation depth errors as a function of the modulation depth error STD σ_χ at 1550 nm. All the studied mode scramblers retain normalized link GD STDs lower than 10, even for the highest modulation depth error STD. The robustness of the mode scramblers to modulation depth errors can be understood by considering the effect of an increase or a decrease in the modulation depth. Deviated mode scramblers with higher modulation depths have larger coupling coefficients between all modes, which enhances inter-group coupling. These mode scramblers compensate for the deviated mode scramblers that have smaller modulation depths, which have smaller coupling coefficients and therefore less inter-group coupling. Fabricating a grating with a particular modulation depth is difficult since measurement of the modulation depth involves inversion from transmission and reflection spectra [31] or advanced optical probing techniques [32]. Therefore, it is helpful that modulation depth errors do not increase link GD STD substantially.

Next, we consider the fabrication error scenarios with systematic errors shown in Fig. 12(d) to (f). Systematic errors increase link GD STD more than random errors since the same error is repeated 100 times along the link.

Fig. 12(d) shows the worst-case normalized link GD STD $\sigma'_{GD}(100)/\sigma_{GD}(1)$ due to systematic RI errors as a function of the RI error STD at 1550 nm. At a RI error STD of 10×10^{-5}, the worst-case link GD STD increases by almost 80% for the $\chi = 20 \times 10^{-5}$ design. Other designs have much larger link GD

STDs, indicating that the worst-case deviated mode scramblers provide weak inter-group coupling. We note that the link GD STD increases more for the $\chi = 15 \times 10^{-5}$ design than the $\chi = 10 \times 10^{-5}$ design. This occurs because the $\chi = 15 \times 10^{-5}$ design uses a longer grating period, which is suboptimal for inter-group coupling, to decrease the mode scrambler loss. If both designs shared the same grating period, fabrication errors would increase the link GD STD of the $\chi = 15 \times 10^{-5}$ design less than that of the $\chi = 10 \times 10^{-5}$ design.

Fig. 12(e) shows the worst-case normalized link GD STD $\sigma'_{\mathrm{GD}}(100)/\sigma_{\mathrm{GD}}(1)$ due to systematic grating period errors as a function of the maximum grating period error δ_Λ at 1550 nm. The impact of systematic grating period errors on link GD STD is also severe. At the highest grating period error, the $\chi = 20 \times 10^{-5}$ design has at most a 25% increase in link GD STD, while other designs degrade by over 80%.

Fig. 12(f) shows the worst-case normalized link GD STD $\sigma'_{\mathrm{GD}}(100)/\sigma_{\mathrm{GD}}(1)$ due to systematic modulation depth errors as a function of the maximum modulation depth error δ_χ at 1550 nm. Systematic errors in the modulation depth are not as problematic as other systematic errors, just as random modulation depth errors are not as problematic as other random errors. At the highest systematic modulation depth error, the link GD STD increases by 30% for the $\chi = 5 \times 10^{-5}$ design.

Fig. 12, in the context of Fig. 8, clearly shows that the choice of modulation depth involves a tradeoff between mode scrambler loss and sensitivity of link GD STD to fabrication errors. While designs with lower modulation depths have lower MDL STDs and MALs, the link GD STD is more sensitive to fabrication errors. Depending on fabrication tolerances, mode scramblers with higher modulation depths may be preferred despite having higher losses. We also observe that systematic errors are more problematic than random errors and, in particular, systematic errors in the transverse index profile or grating period cause substantial increases in link GD STD. One should develop grating period and transverse index profile calibration procedures to minimize systematic error. If a systematic error in the transverse index profile is found, one can redesign the longitudinal grating to minimize the increase of the link GD STD. In general, mode scramblers should be designed with higher modulation depths if systematic errors are unavoidable.

IV. Discussion

We have shown that optimization-based joint design of the transverse index profile and longitudinal grating can yield very low-loss mode scrambler designs that induce sufficient inter-group power coupling to reduce link MDL STD and GD STD over the entire C-band. Here, we comment on extensions that may be addressed in future research and the limitations of our work.

We can use our approach to design mode scramblers for MDM links supporting more mode groups by appropriately changing the set of guided mode indices $\mathcal{M}_{\mathrm{guided}}$, cutoff mode indices $\mathcal{M}_{\mathrm{cutoff}}$, and desired propagation constants β^{des} in the transverse RI optimization objective (13). A uniform grating directly couples modes in adjacent mode groups. As N_g increases, it is more important to have equal propagation constant spacings between mode groups for efficient coupling. Especially for a large N_g, the tradeoff between cutoff mode offset and equal propagation constant spacings, as shown in Fig. 7, may limit performance.

Some mode scrambler designs cause the link GD STD to accumulate more slowly than in a strongly coupled link with a coupling length equal to the span length. For example, all the scrambler designs in Fig. 12, in the absence of errors, achieve a normalized GD STD less than 10 for a $K = 100$ span link, with one design achieving a normalized GD STD of 8.1. An important research direction is to study the mechanism behind this reduced GD STD and the design of LPFG-based mode scramblers with this property. Our optimization-based design method can numerically search for mode scramblers that yield $\sigma_{\mathrm{GD}}(K) < \sqrt{K}\sigma_{\mathrm{GD}}(1)$ by multiplying the denominator of the argument in the first term of (16) by a constant less than one. These devices are most effective when random inter-group coupling is weak [33]. Understanding the effect of random inter-group coupling on the design and performance of these devices is another potential research direction.

Control of the LPFG-based mode scrambler transfer matrix to induce sufficient inter-group power exchange is important in achieving link MDL STD and GD STD reduction. Due to complicated coupling interactions, designing a specific transfer matrix is challenging. Another important research direction is to study the subspace of transfer matrices achievable by a single LPFG or multiple concatenated LPFGs.

Since the designed mode scramblers have low loss, it is possible to use multiple mode scramblers per span. By using K_0 mode scramblers per span, we can reduce the link GD STD and MDL STD by approximately an additional factor of $\sqrt{K_0}$.

LPFGs are also frequently used as refractometers for biomedical and chemical applications [34]. In these applications, the surrounding refractive index (SRI) is modified by the presence of chemical or biological material, causing detectable changes in the transmission spectrum of the LPFG. Enhancing sensitivity to changes in the SRI is critical for sensor applications [34]. An interesting research direction is to use the transverse RI optimization techniques employed here [20] to design sensors with improved SRI sensitivity.

While allowing for free-form optimization of the transverse index profile, we restricted ourselves to a uniform, sinusoidal grating with no chirp. This restriction simplifies fabrication and still yields low-loss designs. Including a grating chirp profile as in reference [14] or apodizing the grating may result in performance benefits.

Fabrication of the optimized transverse index profile is an important challenge. Trench-assisted GI fibers supporting various numbers of modes can be manufactured precisely by employing plasma vapor chemical deposition [35], [36], [37], [38]. Obtaining specialized transverse index profiles as described here may be challenging with existing techniques. Recent developments

in fused silica optical fiber fabrication using nanostructured cores show significant promise in overcoming limitations in fabricating free-form GI fibers [39].

V. Conclusion

We proposed a design strategy for LPFG-based mode scramblers involving joint optimization of the transverse index profile and longitudinal grating. First, optimization of the transverse index profile yields equal spacing between the propagation constants of the guided mode groups and significantly different propagation constant spacings between the highest-order guided modes and the unguided modes. Then, grid search optimization is employed to find a grating design with minimal mode scrambler MDL STD and MAL while ensuring sufficient inter-group coupling so the link MDL STD and GD STD accumulate with the square root of the number of spans.

We used this design strategy to find efficient mode scrambler designs for MDM links supporting $D = 12$ modes, as proposed by Srinivas et al. [7]. We obtained a design with an MDL STD and MAL less than 0.011 dB and 0.027 dB, respectively, over the C-band.

We performed numerical simulations to study the effect of fabrication errors on mode scrambler performance. Random errors in the transverse index profile do not significantly impact the mode scrambler MDL STD and MAL. The link GD STD is robust to modulation depth deviations but is sensitive to grating period deviations and random errors in the transverse index profile. The choice of modulation depth involves a tradeoff between mode scrambler losses and sensitivity of link GD STD to fabrication errors.

Acknowledgment

References

[1] H. Srinivas et al., "Modeling and experimental measurement of power efficiency for power-limited SDM submarine transmission systems," *J. Lightw. Technol.*, vol. 39, no. 8, pp. 2376–2386, Apr. 2021. [Online]. Available: https://ieeexplore.ieee.org/document/9314868

[2] O. V. Sinkin, A. V. Turukhin, W. W. Patterson, M. A. Bolshtyansky, D. G. Foursa, and A. N. Pilipetskii, "Maximum optical power efficiency in SDM-Based optical communication systems," *IEEE Photon. Technol. Lett.*, vol. 29, no. 13, pp. 1075–1077, Jul. 2017. [Online]. Available: https://ieeexplore.ieee.org/document/7919195

[3] O. V. Sinkin et al., "SDM for power-efficient undersea transmission," *J. Lightw. Technol.*, vol. 36, no. 2, pp. 361–371, Jan. 2018.

[4] J.-X. Cai et al., "9 tb/s transmission using 29 mW optical pump power per EDFA with 1.24 tb/s/w optical power efficiency over 15,050 km," *J. Lightw. Technol.*, vol. 40, no. 6, pp. 1650–1657, Mar. 2022. [Online]. Available: https://ieeexplore.ieee.org/document/9626578

[5] W. Klaus et al., "Advanced space division multiplexing technologies for optical networks [Invited]," *J. Opt. Commun. Netw.*, vol. 9, no. 4, pp. C1–C11, Apr. 2017. [Online]. Available: https://ieeexplore.ieee.org/document/7901441

[6] P. J. Winzer, R. Ryf, and S. Randel, "Chapter 10 - Spatial multiplexing using multiple-input multiple-output signal processing," in *Optical Fiber Telecommunications*, 6th ed. Boston, MA, USA: Academic Press, Jan. 2013, pp. 433–490. [Online]. Available: https://www.sciencedirect.com/science/article/pii/B9780123969606000109

[7] H. Srinivas, O. Krutko, and J. M. Kahn, "Efficient integrated multimode amplifiers for scalable long-haul SDM transmission," *J. Lightw. Technol.*, vol. 41, no. 15, pp. 4989–5002, Aug. 2023. [Online]. Available: https://ieeexplore.ieee.org/document/10064021

[8] K.-P. Ho and J. M. Kahn, "Mode coupling and its impact on spatially multiplexed systems," in *Optical Fiber Telecommunications*, Amsterdam, Netherlands: Elsevier, 2013, pp. 491–568. [Online]. Available: https://linkinghub.elsevier.com/retrieve/pii/B9780123969606000110

[9] K.-P. Ho and J. M. Kahn, "Frequency diversity in mode-division multiplexing systems," *J. Lightw. Technol.*, vol. 29, no. 24, pp. 3719–3726, Dec. 2011.

[10] R. V. Jensen, L. Grüner-Nielsen, N. H. L. Wong, Y. Sun, Y. Jung, and D. J. Richardson, "Demonstration of a 9 LP-Mode transmission fiber with low DMD and loss," presented at the Opt. Fiber Commun. Conf., Los Angeles, CA, USA, Mar. 22–26, 2015, Paper W2A.34. [Online]. Available: https://opg.optica.org/abstract.cfm?uri=OFC-2015-W2A.34

[11] R. Ryf et al., "Mode-multiplexed transmission over conventional graded-index multimode fibers," *Opt. Exp.*, vol. 23, no. 1, pp. 235–246, Jan. 2015. [Online]. Available: https://opg.optica.org/oe/abstract.cfm?uri=oe-23-1-235

[12] N. K. Fontaine et al., "Characterization of space-division multiplexing systems using a swept-wavelength interferometer," in *Proc. 2013 Opt. Fiber Commun. Conf. Expo. Nat. Fiber Optic Engineers Conf.*, Mar. 2013, pp. 1–3. [Online]. Available: https://ieeexplore.ieee.org/abstract/document/6533121

[13] S. O. Arik, K.-P. Ho, and J. M. Kahn, "Group delay management and multiinput multioutput signal processing in mode-division multiplexing systems," *J. Lightw. Technol.*, vol. 34, no. 11, pp. 2867–2880, Jun. 2016. [Online]. Available: https://ieeexplore.ieee.org/document/7409913

[14] D. Askarov and J. M. Kahn, "Long-period fiber gratings for mode coupling in mode-division-multiplexing systems," *J. Lightw. Technol.*, vol. 33, no. 19, pp. 4032–4038, Oct. 2015.

[15] Y. Liu, Y. Jung, Z. Yang, L. Zhang, and D. J. Richardson, "Wideband and low-loss mode scrambler for few-mode fibers based on distributed multiple point-loads," *IEEE Photon. J.*, vol. 13, no. 3, Jun. 2021, Art. no. 7100907. [Online]. Available: https://ieeexplore.ieee.org/document/9448421

[16] Y. Zhao, H. Chen, N. K. Fontaine, J. Li, R. Ryf, and Y. Liu, "Broadband and low-loss mode scramblers using CO_2-laser inscribed long-period gratings," *Opt. Lett.*, vol. 43, no. 12, pp. 2868–2871, Jun. 2018. [Online]. Available: https://opg.optica.org/ol/abstract.cfm?uri=ol-43-12-2868

[17] J. Li et al., "Design and demonstration of mode scrambler supporting 10 modes using multiplane light conversion," in *Proc. 2018 Eur. Conf. Opt. Commun.*, Sep. 2018, pp. 1–3. [Online]. Available: https://ieeexplore.ieee.org/document/8535381

[18] Y. Wang, "Review of long period fiber gratings written by CO_2 laser," *J. Appl. Phys.*, vol. 108, no. 8, Oct. 2010, Art. no. 081101. [Online]. Available: https://aip.scitation.org/doi/10.1063/1.3493111

[19] H. Liu et al., "Reducing group delay spread using uniform long-period gratings," *Sci. Rep.*, vol. 8, no. 1, Mar. 2018, Art. no. 3882. [Online]. Available: https://www.nature.com/articles/s41598-018-21609-1

[20] K. Choutagunta and J. M. Kahn, "Designing high-performance multimode fibers using refractive index optimization," *J. Lightw. Technol.*, vol. 39, no. 1, pp. 233–242, Jan. 2021.

[21] J. Meunier and S. Hosain, "An efficient model for splice loss evaluation in single-mode graded-index fibers," *J. Lightw. Technol.*, vol. 9, no. 11, pp. 1457–1463, Nov. 1991. [Online]. Available: https://ieeexplore.ieee.org/document/97632

[22] Y.-C. Lu, W.-P. Huang, and S.-S. Jian, "Full vector complex coupled mode theory for tilted fiber gratings," *Opt. Exp.*, vol. 18, no. 2, pp. 713–726, Jan. 2010. [Online]. Available: https://opg.optica.org/oe/abstract.cfm?uri=oe-18-2-713

[23] J. Fang, A. Li, and W. Shieh, "Low-DMD few-mode fiber with distributed long-period grating," *Opt. Lett.*, vol. 40, no. 17, pp. 3937–3940, Sep. 2015. [Online]. Available: https://opg.optica.org/ol/abstract.cfm?uri=ol-40-17-3937

[24] A. Hale, T. A. Strasser, and P. S. Westbrook, "Optical fiber gratings with index matched polymer coatings for cladding mode suppression," European Patent EP1146357A2, Oct., 2001. [Online]. Available: https://patents.google.com/patent/EP1146357A2/en

[25] K.-P. Ho and J. M. Kahn, "Mode-dependent loss and gain: Statistics and effect on mode-division multiplexing," *Opt. Exp.*, vol. 19, no. 17, pp. 16612–16635, Aug. 2011. [Online]. Available: https://opg.optica.org/oe/abstract.cfm?uri=oe-19-17-16612

[26] S. Fan and J. M. Kahn, "Principal modes in multimode waveguides," *Opt. Lett.*, vol. 30, no. 2, pp. 135–137, Jan. 2005. [Online]. Available: https://opg.optica.org/ol/abstract.cfm?uri=ol-30-2-135

[27] D. Marcuse, "Chapter 2 - Weakly Guiding Optical Fibers," in *Theory of Dielectric Optical Waveguides*, 2nd ed. Cambridge, MA, USA: Academic Press, Jan. 1991, pp. 60–96. [Online]. Available: https://www.sciencedirect.com/science/article/pii/B9780124709515500081

[28] W. W. Morey, G. Meltz, J. D. Love, and S. J. Hewlett, "Mode-coupling characteristics of UV-written Bragg gratings in depressed-cladding fibre," *Electron. Lett.*, vol. 30, pp. 730–732, Apr. 1994. [Online]. Available: https://ui.adsabs.harvard.edu/abs/1994ElL....30..730M

[29] S. J. Hewlett, J. D. Love, G. Meltz, T. J. Bailey, and W. W. Morey, "Cladding-mode coupling characteristics of Bragg gratings in depressed-cladding fibre," *Electron. Lett.*, vol. 31, pp. 820–822, May 1995. [Online]. Available: https://ui.adsabs.harvard.edu/abs/1995ElL....31..820H

[30] G. Agrawal, "*Fiber-Optic Communication Systems* (Microwave and Optical Engineering Series). Hoboken, NJ, USA: Wiley, 2012.

[31] E. Brinkmeyer, "Simple algorithm for reconstructing fiber gratings from reflectometric data," *Opt. Lett.*, vol. 20, no. 8, pp. 810–812, Apr. 1995. [Online]. Available: https://opg.optica.org/ol/abstract.cfm?uri=ol-20-8-810

[32] P. A. Krug, R. Stolte, and R. Ulrich, "Measurement of index modulation along an optical fiber Bragg grating," *Opt. Lett.*, vol. 20, no. 17, pp. 1767–1769, Sep. 1995. [Online]. Available: https://opg.optica.org/ol/abstract.cfm?uri=ol-20-17-1767

[33] A. Vijay, O. Krutko, R. Refaee, and J. M. Kahn, "Modal statistics in mode-division-multiplexed systems using mode scramblers," *J. Lightw. Technol.*, early access, Sep. 20, 2024, doi: 10.1109/JLT.2024.3466009. [Online]. Available: https://ieeexplore.ieee.org/document/10685071/?arnumber=10685071

[34] J. Cai, Y. Liu, and X. Shu, "Long-period fiber grating sensors for chemical and biomedical applications," *Sensors*, vol. 23, no. 1, Jan. 2023, Art. no. 542. [Online]. Available: https://www.mdpi.com/1424-8220/23/1/542

[35] P. Sillard, D. Molin, M. Bigot-Astruc, H. Maerten, D. V. Ras, and F. Achten, "Low-DMGD 6-LP-mode fiber," presented at the Opt. Fiber Commun. Conf., San Francisco, CA, USA, Mar. 9–13, 2014, Paper M3F.2. [Online]. Available: https://opg.optica.org/abstract.cfm?uri=OFC-2014-M3F.2

[36] P. Sillard, "Few-mode fibers for space division multiplexing," in *Proc. 2016 Opt. Fiber Commun. Conf. Exhib.*, Mar. 2016, pp. 1–53. [Online]. Available: https://ieeexplore.ieee.org/document/7537334

[37] P. Sillard et al., "Low-differential-Mode-Group-Delay 9-LP-Mode fiber," *J. Lightw. Technol.*, vol. 34, no. 2, pp. 425–430, Jan. 2016. [Online]. Available: https://ieeexplore.ieee.org/document/7174947

[38] P. Sillard et al., "Few-mode fiber technology, deployments, and systems," *Proc. IEEE*, vol. 110, no. 11, pp. 1804–1820, Nov. 2022. [Online]. Available: https://ieeexplore.ieee.org/document/9906979

[39] A. Anuszkiewicz et al., "Fused silica optical fibers with graded index nanostructured core," *Sci. Rep.*, vol. 8, no. 1, Aug. 2018, Art. no. 12329. [Online]. Available: https://www.nature.com/articles/s41598-018-30284-1

Oleksiy Krutko (Student Member, IEEE) received the B.S. degree in electrical engineering from the University of Texas at Austin, Austin, TX, USA, in 2020. He is currently working toward the Ph.D. degree with Stanford University, Stanford, CA, USA. His research interests include optical fiber communications and photonic devices.

Rebecca Refaee received the B.S. degree in mathematics and the M.S. degree in electrical engineering in 2024 from Stanford University, Stanford, CA, USA, where she is currently working toward the Ph.D. degree in electrical engineering. Her research interests include optical communications and mode-division multiplexing.

Anirudh Vijay (Member, IEEE) received the B.Tech. and M.Tech. degrees in electrical engineering from the Indian Institute of Technology Madras, Chennai, Tamil Nadu, India, in 2019. He is currently working toward the Ph.D. degree in electrical engineering with Stanford University, Stanford, CA, USA. His research interests include optical communications, mode-division multiplexing, and data-center applications.

Joseph M. Kahn (Life Fellow, IEEE) received the A.B., M.A., and Ph.D. degrees in physics from the University of California, Berkeley, CA, USA, in 1981, 1983, and 1986, respectively. From 1987 to 1990, he was with AT&T Bell Laboratories. In 1989, he demonstrated the first successful synchronous (i.e., coherent) detection using semiconductor lasers, achieving record receiver sensitivity. From 1990 to 2003, he was on the Electrical Engineering and Computer Sciences Faculty in Berkeley. In 1992, he demonstrated coherent detection of QPSK. In 1999, D. S. Shiu and Kahn has authored or coauthored the first work on probabilistic shaping for optical communications. In the 1990s and early 2000s, he and collaborators performed seminal work on indoor and outdoor free-space optical communications and multi-input multi-output wireless communications. In 2000, Kahn and K. P. Ho founded StrataLight Communications, whose 40 Gb/s-per-wavelength long-haul fiber transmission systems were deployed widely by AT&T, Deutsche Telekom, and other carriers. In 2002, Ho and Kahn applied to patent the first electronic compensation of fiber Kerr nonlinearity. In 2009, StrataLight was acquired by Opnext. In 2003, he became a Professor of electrical engineering with E. L. Ginzton Laboratory, Stanford University, Stanford, CA, USA. He and collaborators have extensively studied rate-adaptive coding and modulation, as well as digital signal processing for mitigating linear and nonlinear impairments in coherent systems. In 2008, E. Ip and Kahn (and G. Li independently) invented simplified digital backpropagation for compensating fiber Kerr nonlinearity and dispersion. Since 2004, he and collaborators have studied propagation, modal statistics, spatial multiplexing and imaging in multimode fibers, elucidating principal modes and demonstrating transmission beyond the traditional bandwidth-distance limit in 2005, deriving the statistics of coupled modal group delays and gains in 2011, and deriving resolution limits for imaging in 2013. His research interests include optical frequency comb generators, coherent data center links, rate-adaptive access networks, fiber Kerr nonlinearity mitigation, ultra-long-haul submarine links, and optimal free-space transmission through atmospheric turbulence. He was the recipient of the National Science Foundation Presidential Young Investigator Award in 1991. In 2000, he became a Fellow of the IEEE.